Nonalloying surface reconstructions of ultrathin Sn films on Cu(111) investigated with LEED, XPS, and photoelectron extended fine structure analysis

Xihui Liang,[1,2] Jun-Hao Deng,[1] Liang-Jen Fan,[3] Yaw-Wen Yang,[3] and Dah-An Luh[1,3,*]

[1]*Department of Physics, National Central University, Taoyuan 32001, Taiwan*

[2]*Guangzhou Research Institute of Optics-Mechanics-Electricity Technology, Guangzhou 510663, P. R. China*

[3]*National Synchrotron Radiation Research Center, Hsinchu 30076, Taiwan*

(Received 18 February 2011; revised manuscript received 26 May 2011; published 2 August 2011)

By preventing surface alloying during growth of Sn on Cu(111) at 100 K, we discovered two novel nonalloying surface reconstructions, denoted as lower-coverage (LC) and higher-coverage (HC) phases. They were investigated with low energy electron diffraction (LEED), x-ray photoemission spectroscopy (XPS), and analysis of photoelectron extended fine structure (PEFS). The LC phase has a p(2 × 2) structure with one Sn atom per unit cell, corresponding to a Sn coverage 0.25 ML; the HC phase has a structure of $\mathbf{M} = \begin{pmatrix} 2 & 1 \\ 1 & 3 \end{pmatrix}$ (matrix notation) with two Sn atoms per unit cell, corresponding to a Sn coverage 0.40 ML. Structural models for the two phases are proposed.

DOI: 10.1103/PhysRevB.84.075406 PACS number(s): 68.55.−a, 61.05.jh, 79.60.Dp

I. INTRODUCTION

Controlling the growth of nanoscale structures is a fundamental task in research on nanotechnology and surface science. The deposition of one metal on the surface of another metal to form thin films or alloy has been widely exploited to modify or to create novel-surface properties,[1] which offers a way to investigate the formation of nanoscale structures and to develop a capability of manipulating matter on a nanometer scale.[2] Among numerous bimetallic systems, the Sn-Cu alloys, known as bronzes, have drawn much attention because of their important role in the development of early civilizations. Because of the large difference in the sizes of Sn and Cu atoms, the surface of the Sn-Cu system possesses diverse properties and is commonly utilized as a model system to investigate the dynamics of formation of heteroepitaxial films and surface alloys. The deposition of Sn on Cu(100) has been extensively investigated, and numerous ordered phases were identified with a submonolayer coverage.[3–7] In contrast to Sn/Cu(100), fewer phases were discovered in the Sn/Cu(111) system. No well-defined surface structure is identified when Sn is deposited on Cu(111) at 300 K, and subsequent annealing produces a surface with the p($\sqrt{3} \times \sqrt{3}$)−R30° structure, called the $\sqrt{3}$ phase in what follows, through the formation of a stable two-dimensional Sn-Cu alloy on incorporating the Sn atoms into the uppermost layer of the Cu(111) surface.[3,8]

The alloying mechanism of Sn on Cu(111) attracted renewed attention when the migration of reactive Sn islands on Cu(111) was reported. Large, two-dimensional Sn islands on Cu(111) travel across the Cu(111) surface, leaving behind traces of surface alloys.[9] The speed of the traveling Sn islands, which is closely related to the rate of surface alloying, varies over several orders of magnitude, on altering slightly the substrate temperature near 300 K from ∼1000 nm/s at 350 K to ∼10 nm/s at 300 K to ∼0.1 nm/s at 260 K.[9] This dependence of the speed of the Sn islands migrating on Cu(111) indicates that the alloying of Sn into Cu(111) is almost completely preventable on lowering the substrate temperature.

In this work we investigated the growth of ultrathin Sn layers on Cu(111) under conditions of little or no surface alloying. On depositing Sn on Cu(111) at low temperature, we uncovered two novel nonalloying ordered surface reconstructions: a lower-coverage (LC) phase and a higher-coverage (HC) phase. Both phases were investigated with low energy electron diffraction (LEED), x-ray photoemission spectroscopy (XPS), and analysis of photoemission extended fine structure (PEFS). Based on the results from our analyses, we propose structural models for the two phases. The fact that novel-ordered surface structures can result from the growth at a lower temperature justifies reinvestigations of many well-studied thin-film systems, especially those forming surface alloys near 300 K.

II. EXPERIMENTS

The experiments were performed at an end station attached to the wide-range spherical-grating beamline (BL24A) at National Synchrotron Radiation Research Center, Taiwan. The end station is an ultrahigh-vacuum mu-metal chamber with the base pressure less than 5×10^{-10} Torr. The end station houses a LEED instrument, a differentially pumped ion gun for sample cleaning, an electron-energy analyzer (SPECS PHOIBOS 150) for measurements of XPS and angle-resolved photoemission spectra, and an evaporator for Sn deposition. A Cu(111) single crystal (diameter 1 cm) is mounted at the bottom of a manipulator containing electrical and liquid nitrogen feedthroughs; the sample temperature, measured with a thermocouple junction (type K) attached directly on the sample, is variable from 100 to 1000 K. The Cu(111) surface was cleaned with Ar-ion sputtering and annealing in repeated cycles until a sharp p(1 × 1) LEED pattern and the Shockley surface state[10] were obtained. Tin was evaporated from a crucible heated with electron bombardment; the same evaporating conditions were used throughout the experiment. The rate of deposition was ∼0.04 ML/min, as calibrated with a quartz-crystal microbalance (on another vacuum system) and with the coverage-dependent reconstructions of Sn/Ge(111)[11,12] (on the same vacuum system). Here 1.0 ML is referred to as 1.77×10^{15} atoms/cm^2 required to form one complete Cu(111) surface layer. The relative error of the rate of deposition was less than 15%. The photoemission spectra were recorded with

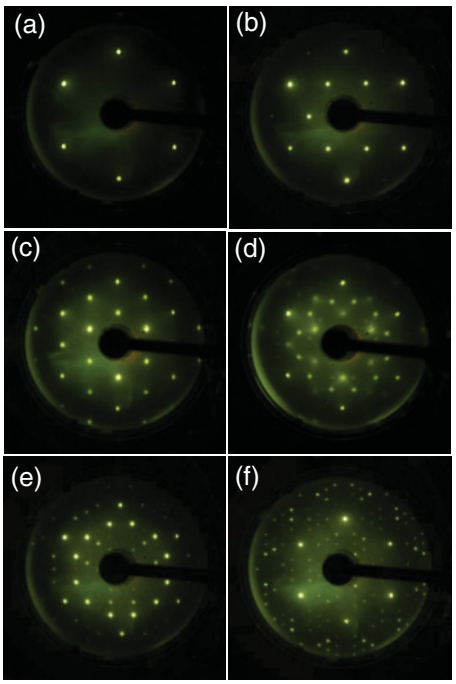

FIG. 1. (Color online) LEED patterns of (a) clean Cu(111) [p(1 × 1)]; (b) $\sqrt{3}$ phase [1/3 ML Sn/Cu(111), p($\sqrt{3} \times \sqrt{3}$)−R30°]; (c) LC phase [0.12 ML Sn/Cu(111), p(2 × 2)]; (d) mixed phase [0.28 ML Sn/Cu(111)]; (e) and (f) HC phase [0.40 ML Sn/Cu(111), three domains of the (2113) structure]. All patterns were measured with electron energy 106 eV, except (f) at 170 eV.

the axis of the acceptance cone normal to the sample surface; the photon beam impinged on the sample with incident angle 45° from the surface normal. The photon energy employed was varied from 20 to 160 eV with energy resolution less than 30 meV. A digital camera remotely controlled through a computer was used to record the LEED patterns. The intensity of diffraction spots in the LEED patterns was modulated strongly with the kinetic energy of the incident electrons; the electrons with varied kinetic energies served to reveal all diffraction spots in each LEED measurement.

III. RESULTS AND DISCUSSION

A. LEED

Figure 1 shows typical LEED patterns of the various surface structures observed on Sn/Cu(111). All LEED patterns in the figure were recorded with electrons of energy 106 eV, except Fig. 1(f) acquired with electrons of energy 170 eV. A sharp LEED pattern of a p(1 × 1) structure was observed for clean Cu(111) [Fig. 1(a)]. The LEED pattern of clean Cu(111) remained p(1 × 1) when the temperature was lowered to 100 K (the lowest temperature achieved in this study). The deposition of Sn on Cu(111) at ∼300 K resulted in a diffuse LEED pattern with a strong background, sometimes mixed with faint spots of a p($\sqrt{3} \times \sqrt{3}$)−R30° structure (image not shown). After the sample was annealed at 550 K, the surface had a sharp LEED pattern of the p($\sqrt{3} \times \sqrt{3}$)−R30° structure [Fig. 1(b)]. Preceding work with ion-scattering and LEED showed that, in this $\sqrt{3}$ phase, the Sn atoms incorporate into the uppermost layer of Cu(111); the ratio of the populations of Cu and Sn is 2, corresponding to 1/3-ML Sn on the surface.[8] These results are insensitive to the Sn coverage. From our LEED observations, for a Sn coverage above 0.25 ML, annealing the sample at 550 K invariably results in the $\sqrt{3}$ phase. Excess Sn likely diffuses into the bulk Cu, leaving a two-dimensional surface alloy on the surface.[8]

As mentioned in the Introduction, surface alloying between Sn atoms and the Cu(111) substrate is preventable on lowering the substrate temperature.[9] To explore the initial growth of Sn on Cu(111) without surface alloying, we deposited Sn (∼0.04 ML) repetitively with the sample at 100 K; the sample was characterized with LEED and XPS at 100 K after each deposition without further treatment, such as annealing. The result differed strongly from the one with deposition at 300 K, and two novel phases were uncovered. Figures 1(c)–1(f) shows representative LEED patterns to illustrate how the surface evolves with increasing Sn coverage. The Sn coverages are in Figs. 1(c) 0.12, (d) 0.28, (e) 0.40, and (f) 0.40 ML. For Sn coverage between 0.04 and 0.20 ML, the surface has a sharp LEED pattern [Fig. 1(c)], called the LC phase. For a Sn coverage between 0.36 and 0.44 ML, the surface shows another sharp LEED pattern [Fig. 1(e)], called the HC phase. Because the intensity of the LEED spots is strongly modulated with the kinetic energy of the incident electrons, some diffraction spots show little or no intensity in Fig. 1(e). Acquiring the LEED patterns with the electrons of varied kinetic energy reveals these missing spots; a LEED pattern better representing the order of the HC phase is shown in Fig. 1(f). For a Sn coverage from 0.20 to 0.36 ML, the surface seems to transform gradually from the LC phase to the HC phase with an apparent coexistence of the two, as implied by the mixed LEED patterns [Fig. 1(d)]. Moreover, the LEED pattern of the HC phase becomes fuzzy when the Sn coverage attains 0.52 ML (image not shown). For a further increased Sn coverage, the LEED pattern becomes fuzzier with a strong background.

The structural periodicity of the surface in the various phases was investigated with software LEEDpat.[13] Figure 2 shows the simulated LEED patterns and the corresponding

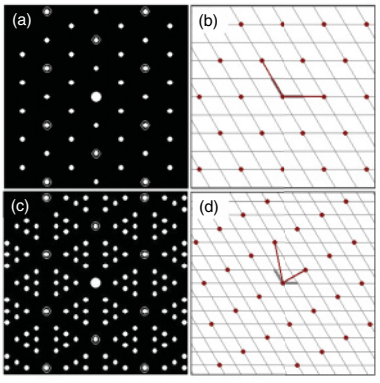

FIG. 2. (Color online) (a) Simulated LEED pattern of p(2 × 2); (b) p(2 × 2) superlattice; (c) simulated LEED pattern of three domains of the (2113) superlattice; (d) (2113) superlattice. In (a) and (c) the spots corresponding to p(1 × 1) are circled. In (b) and (d) the grids show the lattice of p(1 × 1); red line segments are basis vectors and red dots are lattice points of the superlattice.

superlattices. In Figs. 2(a) and 2(c) the simulated LEED spots are indicated as white spots; the spots corresponding to p(1 × 1) are circled. In Figs. 2(b) and 2(d), the grids show a lattice p(1 × 1); the red line segments are the basis vectors and the red dots are the lattice points of the superstructure. Figure 2(a), generated from the p(2 × 2) structure [Fig. 2(b)], matches the LEED pattern of the LC phase [Fig. 1(c)]. Because the LC phase shows the sharpest LEED pattern with Sn coverage ∼0.2 ML, one Sn atom is indicated per unit cell of this p(2 × 2) structure. Both the p(2 × 2) structure and three domains of the p(2 × 1) structure generate a LEED pattern resembling Fig. 1(c), but the p(2 × 1) structure is excluded for the following reasons. The LC phase exists solely with a Sn coverage less than 0.2 ML and coexists with the HC phase with the Sn coverage no more than 0.36 ML, which is much less than 0.5 ML required to form a complete atomic layer of the p(2 × 1) structure with one Sn atom per unit cell. Moreover, the interatomic distances of Sn and Cu in their elemental forms are 2.81 and 2.55 Å, respectively, which enables a rough estimate that the Sn atom is about 10% bigger than the Cu atom. The Sn atoms are unlikely so closely packed to form the p(2 × 1) structure, especially when the LC phase is observed with a Sn coverage as small as 0.04 ML. The LEED pattern of the HC phase [Figs. 1(e) and 1(f)] comprises groups of six spots arranged in triangles with the spots of the p(1 × 1) structure. These LEED patterns satisfactorily match the simulated pattern [Fig. 2(c)] generated from three domains of the structure with $\mathbf{M} = \begin{pmatrix} 2 & 1 \\ 1 & 3 \end{pmatrix}$ (matrix notation), with the basis vectors shown in Fig. 2(d); this superstructure is denoted as the (2113) structure. The Sn coverages required to form a complete atomic layer of the (2113) structure are 0.2, 0.4, and 0.6 ML with 1, 2, and 3 Sn atoms per unit cell. The surface generated the sharpest LEED pattern of the HC phase at ∼0.4 ML, indicating two Sn atoms per unit cell of the (2113) structure for the surface in the HC phase.

B. XPS

The results from the XPS measurements are summarized in Fig. 3. Figure 3(a) shows representative photoemission spectra of the Sn 4*d* core level at various stages of the film growth; the spectra were measured with Sn coverages 0.12, 0.24, and 0.44 ML, corresponding to surfaces of LC, mixed, and HC phases, respectively. All spectra in the figure were measured with photons of 101.6 eV; they have zero binding energy at the Fermi level and are shifted vertically without scaling. Each spectrum comprises a doublet with an asymmetric line shape. With increasing Sn coverage, the asymmetry and the width of the line seem to alter slightly, but no additional core levels with distinct chemical shifts in the binding energy are resolved, which indicates that the chemical environment of the Sn atoms alters unsubstantially when the film is in varied phases. The intensity of the Sn 4*d* core level increases with increasing Sn coverage. To determine the relation between the integrated intensity (area under the curve) of the Sn 4*d* core level and the Sn coverage, each spectrum was fitted to the sum of a doublet consisting of two asymmetric Voigt line shapes and a polynomial background. During fitting, the spin-orbit splitting remained constant; other parameters, such as the branching ratio, the asymmetry of the line shape, the

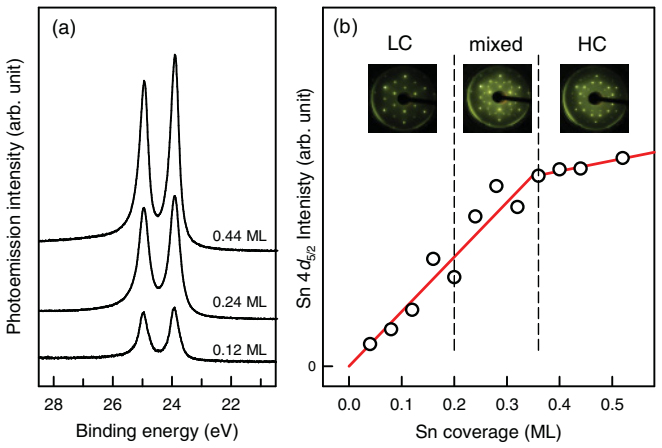

FIG. 3. (Color online) (a) Representative photoemission spectra of the Sn 4*d* core level measured from Sn/Cu(111) of varied Sn coverages. All spectra were measured with photons of energy 101.6 eV. (b) Intensity of the Sn $4d_{5/2}$ core level as a function of Sn coverage (open circles). The figure is divided into regions with vertical dashed lines; each region is labeled with its corresponding LEED pattern. The red lines are the results from linear regression of the data below and above 0.36 ML.

Lorentzian widths, and the Gaussian widths were either set to proper values or left free to vary; the various fitting settings produced results with imperceptible differences. Figure 3(b) shows the intensity of the Sn $4d_{5/2}$ core level as a function of the Sn coverage. According to their LEED patterns, the figure is divided into regions with vertical dashed lines. The intensity of the Sn $4d_{5/2}$ core level increases with increasing Sn coverage; its dependence on the Sn coverage is roughly linear with a break point at ∼0.36 ML. The dependence is illustrated with linear regression of the data below and above 0.36 ML; the results from these regressions are plotted as the red lines in Fig. 3(b). The linear regression of the data of lower coverage is constrained to pass the origin. The varied dependence on the Sn coverage indicates that all deposited Sn atoms stay on the uppermost layer of the surface for Sn coverage less than 0.36 ML; for a Sn coverage exceeding 0.36 ML some Sn atoms begin to remain on top of other Sn atoms. This result indicates that all Sn atoms in both LC and HC phases are on the top of the surface and form a film of thickness one atomic layer.

C. The PEFS analysis

The LC and HC phases were further analyzed with PEFS, which employs the diffraction of photoelectrons to determine the atomic structure surrounding a selected chemical species.[14–19] In addition to the LC and HC phases, the PEFS analysis was also applied to the well-studied $\sqrt{3}$ phase for comparison. After the desired structures with sharp corresponding LEED patterns were obtained, the Sn 4*d* core level was measured with photon energy in a range from 58 to 162 eV. For each phase, 34 spectra were measured. The intensity of the Sn $4d_{5/2}$ core level in each spectrum was calculated with the fitting procedure described in the preceding section. Figure 4(a) shows photoemission intensities of the Sn $4d_{5/2}$ core level as functions of kinetic energy of photoelectrons from various surface structures. At first glance the photoemis-

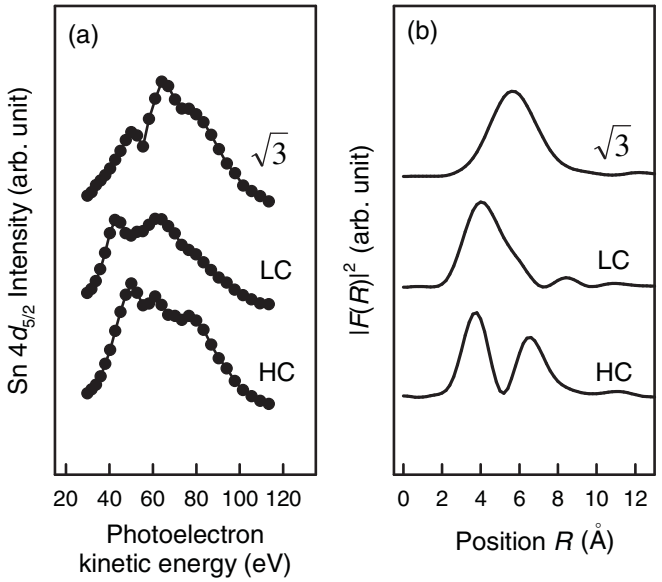

FIG. 4. (a) Photoemission intensities of the Sn $4d_{5/2}$ core level as functions of the photoelectron kinetic energy from various phases of Sn/Cu(111). (b) Position distributions of the scatterer (Cu atom) directly below the photoelectron emitter (Sn atom) for the three phases.

sion intensities in all cases show similar variations: as the photoelectron kinetic energy increases, the intensities at first increase, attain maxima, and then decrease. The photoemission intensity of the Sn $4d_{5/2}$ core level is closely related to both the flux of the incident photons and the photoionization cross section of the Sn $4d_{5/2}$ core level. A similar overall variation in the photoemission intensities is expected, but distinct oscillatory modulations of the photoemission intensities were noticed. These modulations result from interference between the direct photoelectrons and the photoelectrons scattered by the atomic structure surrounding the emitter (or the atom emitting a photoelectron).[14–19] Similar to Ref. 19, all our spectra were measured in a direction normal to the sample surface with a small acceptance angle; the modulation of the photoemission intensity was dominated by backscattering from atoms located directly behind the emitter at a path difference $2R$; R is the distance between the emitter and the scatterer.[19] The modulations of the photoemission intensity $I(k)$ were extracted on calculating the so-called χ function: $\chi(k) = (I(k) - I_0(k))/I_0(k)$; $I_0(k)$ is a smooth background function; and k is the wave vector of photoelectrons. The χ functions were then transformed with respect to the path difference to obtain the distribution functions of the scatterer position,

$$F(R) = \int_{k_{\min}}^{k_{\max}} \chi(k) e^{i2kR} g(k) k dk, \qquad (1)$$

in which $g(k)$ is a window function to avoid truncation errors from a finite k range. The calculated distribution functions $|F(R)|^2$ are shown as solid lines in Fig. 4(b). The distribution functions exhibit one or two dominant features with maxima corresponding to the positions of the scatterers. For the $\sqrt{3}$ phase, one scatterer is located at ~6 Å. Because the nominal spacing between atomic layers normal to the Cu(111) surface is ~2.08 Å, the scatterer (Cu atom) is about three atomic layers below the emitter (Sn atom). For the LC phase one scatterer is located at ~4 Å, about two atomic layers below the emitter. For the HC phase, two scatterers are located at ~3.8 and ~6.3 Å, which are about two and three atomic layers below the emitter, respectively. The strength of a PEFS analysis lies in its sensitivity to surface chemical composition and its ability to sense the atomic structure below the surface, but not in a precise determination of the scatterer position. Without an energy-dependent phase shift included in the transformation, the distribution function is smeared and distorted.[15,16,18] In addition various choices of $I_0(k)$ and $g(k)$ might cause the calculated scatterer positions to shift slightly. Nevertheless, many options were tested in the transformation; the fluctuation in the scatterer positions is a few tenths of 1 Å, which is smaller than the interlayer spacing (~2.08 Å). The scatterer positions determined in Fig. 4(b) are thus subject to error, but the derived relation between the scatterer positions and the inter-layer spacing remains correct.

D. Structural Models

From all information gathered from our experiments, structural models of the various phases of Sn/Cu(111) are derived as shown in Fig. 5. Figures 5(a), 5(c), and 5(e) are top views of the structures; Figs. 5(b), 5(d), and 5(f) are perspective views. In each figure the Sn atoms are depicted as grey spheres. Several atomic layers of the Cu atoms are depicted as yellow spheres of varied brightness; Cu atoms of lighter hue are nearer the surface. Some bonds between neighboring atoms are drawn to improve the presentation of the locations of atoms. Red parallelograms in Figs. 5(a), 5(c), and 5(e) indicate one unit cell of the superstructures. The vertical blue dashed lines, drawn normal to the Cu(111) surface, connect the photoelectron emitter (Sn atom) to the scatterer (Cu atom) that plays the dominant role in causing the intensity modulation in our PEFS measurement. The proposed structural models for the LC and HC phases are based on the assumption of no surface alloying of Sn on Cu(111). Schmid *et al.* suggested that the surface alloying of Sn on Cu(111) is prevented almost completely at 260 K.[9] The Sn substitution of Cu on the first layer of Cu(111) is unlikely when the sample temperature is kept at 100 K. Figure 5 is meant to provide qualitative illustrations of the structures. As mentioned previously, PEFS analysis does not yield precise bond lengths in general. Surface reconstruction is typically accompanied with structural relaxation, of which the determination is beyond the capability of the techniques that we employed. The structural models proposed here nevertheless provide an effective initial point for further quantitative studies with other techniques, such as surface x-ray diffraction and structural optimization of a calculation from first principles.

1. The $\sqrt{3}$ phase

The commonly accepted structural model of the $\sqrt{3}$ phase, studied previously, is shown in Figs. 5(a) and 5(b). The preceding ion-scattering experiment showed that, in this phase, Sn atoms become incorporated into the uppermost layer of the Cu(111) surface to form a two-

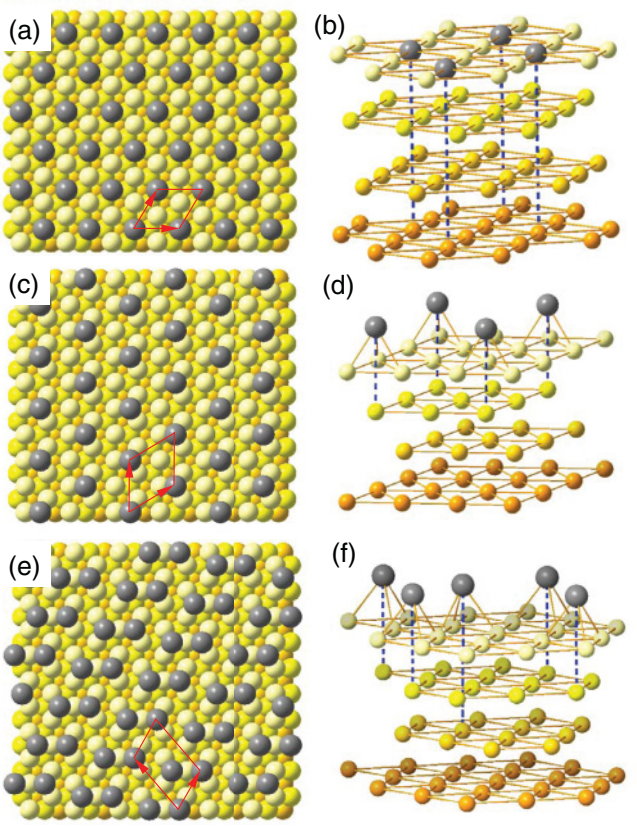

FIG. 5. (Color online) Proposed structural models of phases of Sn/Cu(111). (a) Top view and (b) perspective view of $\sqrt{3}$ phase. (c) Top view and (d) perspective view of LC phase. (e) Top view and (f) perspective view of HC phase. Grey balls denote Sn atoms, and others are the Cu atoms. Cu atoms in varied layers are illustrated with varied hue. Red parallelograms in (a), (c), and (e) indicate one unit cell of the superstructure. Drawn normal to the surface, the vertical blue dashed lines in (b), (d), and (f) connect Sn atoms to Cu atoms directly below.

dimensional surface alloy, with ratio Cu/Sn = 2 of the populations.[8] Because of the fcc stacking, a Cu atom is located three atomic layers directly below the Sn atom, as indicated with blue lines in Fig. 5(b). This observation agrees satisfactorily with the result derived from Fig. 4(b) and confirms the validity of our PEFS analysis.

2. The LC phase

The LC phase, which has the p(2 × 2) structure, has not been studied previously. Schmid *et al*. mentioned the first observation of a p(2 × 2) structure on the surface of Sn islands migrating on Cu(111)[9] but performed no further investigation on it. Our result indicates one Sn atom per unit cell of the p(2 × 2) structure, corresponding to 0.25-ML Sn on Cu(111). In addition our PEFS analysis indicates that a Cu atom is located two atomic layers directly below the Sn atom. Several possible adsorption sites on Cu(111) for the Sn atom include: on top of a Cu atom (T), a bridge site between two neighboring Cu atoms (B), and three-fold hollow sites with a Cu atom (H_1) and without a Cu atom (H_2) one atomic layer below the Cu(111) surface; they are labeled on the right side of Fig. 6. Our result indicates that the Sn atom adsorbs on

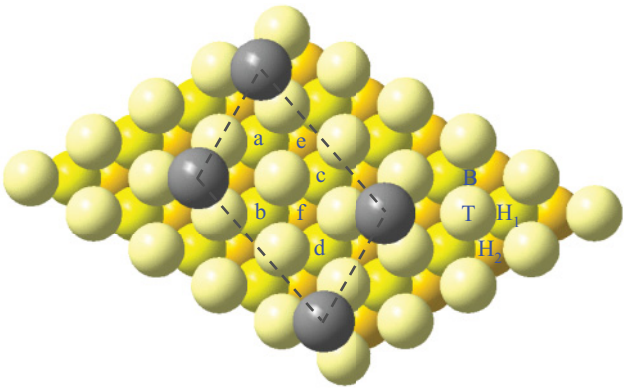

FIG. 6. (Color online) Structural model of Sn/Cu(111). Adsorption sites on Cu(111) are labeled with T (top site), B (bridge site), H_1 (three-fold hollow site with a Cu atom one atomic layer beneath the surface), and H_2 (three-fold hollow site with a Cu atom two atomic layers beneath the surface). One unit cell of the (2113) superlattice is indicated with dashed lines, with Sn atoms (the grey balls) occupying H_1 sites at corners of the unit cell. Some three-fold hollow sites within the unit cell are labeled with a–f.

the H_1 site; the structural model is shown in Figs. 5(c) and 5(d). This model agrees with the result from a theoretical calculation in which Yu *et al*. investigated the adsorption of Sn atoms on Cu(111).[20] Their result shows that the H_1 site is the most energetically favorable. Despite the H_2 site being less energetically favorable, the difference of adsorption energies between the two sites is only 28 meV.

3. The HC phase

The HC phase was not observed previously. Our result indicates two Sn atoms per unit cell of the (2113) structure, corresponding to 0.40 ML Sn on Cu(111). Our PEFS analysis shows Cu atoms to be located two and three atomic layers directly below Sn atoms, indicating that Sn atoms adsorb on the H_1 and H_2 sites, respectively. A structural model to fulfill all experimental observations is proposed in Figs. 5(e) and 5(f). In each unit cell one Sn atom occupies the H_1 site and another occupies the H_2 site. A question arises why, as there are several H_1 sites available in each unit cell, both Sn atoms do not occupy these H_1 sites, which seem the most energetically favored theoretically.[20] There are five H_1 sites and five H_2 sites in each unit cell of the (2113) structure. Figure 6 shows one unit cell of the (2113) structure on Cu(111), indicated with dashed lines, with one Sn atom already occupying the H_1 site. Some three-fold hollow sites are labeled; three H_2 sites in the unit cell are not labeled because they are too near the adsorbed Sn atom to be occupied by a second Sn atom. When a second Sn atom occupies sites a–d (the H_1 sites) and sites e and f (the H_2 sites), the distances between two Sn atoms are $d_{\mathrm{Cu-Cu}}$ and $4/3d_{\mathrm{Cu-Cu}}$, respectively; $d_{\mathrm{Cu-Cu}} \sim 2.55$ Å is the distance between Cu atoms. The preceding calculation predicted that adsorption of the Sn atom on Cu(111) favors the H_1 site over the H_2 site, but the energy difference between the two is small (28 meV).[20] As mentioned previously, the Sn atom is roughly 10% larger than the Cu atom. When the Sn coverage increases, the Sn atoms likely approach so near each other that the interaction between these Sn atoms makes

it energetically unfavored for both Sn atoms to occupy the H_1 sites in each unit cell. Further theoretical analyses with a larger Sn coverage on Cu(111) are necessary to clarify this issue.

Two H_2 sites (sites e and f) are equivalent in the sense that the surface has the same energy and generates the same LEED pattern when the second Sn atom occupies either of them, but the two sites cannot be related through operations of translation and rotation on the surface lattice. Considering the three-fold symmetry of the surface, up to six equivalent structures thus coexist in the HC phase. The techniques with large probing sizes, such as the LEED and XPS in this work, deliver only mixed signals of all structures, but techniques utilizing scanning probes with atomic resolution might resolve the domains with distinct equivalent structures on the surface of the HC phase.

E. Nonequilibrium growth at low temperature

The discovery of two novel ordered phases with growth at low temperature was unexpected. Overbury and Ku investigated the surface of Sn/Cu(111) with alkaline ion scattering and LEED and stated explicitly that a $p(2 \times 2)$ structure was not observed.[8] Aguilar *et al*. performed Monte-Carlo simulations and concluded that Sn atoms are almost entirely incorporated into the uppermost surface plane of Cu(111) to form the $\sqrt{3}$ phase even at 100 K,[3] which apparently contradicts the experimental results reported here. The LC and HC phases of Sn/Cu(111) were not observed previously likely because the growth of Sn on Cu(111) was performed at or above ~300 K, at which the effect from surface alloying is significant.[9] With the prevention of surface alloying between Sn and the Cu(111) substrate at low temperature, Sn atoms are able to stay on top of Cu(111) to form ordered structures. A low temperature is traditionally avoided during film growth because of the decreased mobility of surface atoms. The idea behind the growth at low temperature is to grow the film in a nonequilibrium process. Instead of proceeding to the most stable state directly, the system is trapped in a metastable state because of the limited energy available to the system. Our result indicates that revisiting thin-film systems with growth at low temperature might be worthwhile, especially for those thin-film systems that form surface alloys near 300 K and of which the surface atoms remain mobile at a lower temperature.

IV. SUMMARY

By decreasing the temperature of the Cu(111) surface during growth of ultrathin Sn films, we discovered two nonalloying surface phases, the LC and HC phases. These two phases, together with the $\sqrt{3}$ phase, were investigated with LEED, XPS, and the PEFS analysis, and their structural models are proposed. The ideal LC phase has a Sn coverage 0.25 ML and a $p(2 \times 2)$ structure, with one Sn atom per unit cell occupying the H_1 site. The ideal HC phase has a Sn coverage 0.40 ML and the (2113) structure, with two Sn atoms per unit cell; one Sn atom occupies the H_1 site and the other occupies the H_2 site. The physical and chemical properties of these novel reconstructions require future investigation with other experimental and theoretical approaches, such as scanning probe microscopy, surface x-ray diffraction, and theoretical calculation. The success of our growth at low temperature encourages revisiting other thin-film systems of which the film growth has not been investigated at low temperature.

ACKNOWLEDGMENTS

The authors give thanks to the National Science Council, Taiwan (Grants No. NSC97-2112-M-008-018-MY2 and No. NSC99-2811-M-008-068) and the National Synchrotron Radiation Research Center, Taiwan for providing financial support.

*Corresponding author: luh.dah.an@gmail.com

[1] M. Wuttig and X. Liu, *Ultrathin Metal Films: Magnetic and Structural Properties* (Springer, Berlin Germany 2004), p. 2.

[2] D. H. Lowndes, ed., *Nanoscale Science, Engineering and Technology Research Directions* (Oak Ridge National Laboratory, Oak Ridge, TN, USA, 1999), p. 27.

[3] J. F. Aguilar, R. Ravelo, and M. I. Baskes, Modelling Simul. Mater. Sci. Eng. **8**, 335 (2000).

[4] E. McLoughlin, A. A. Cafolla, E. Al-Shamaileh, and C. J. Barnes, Surf. Sci. **482–485**, 1431 (2001).

[5] A. A. Cafolla, E. McLoughlin, E. Al-Shamaileh, P. Guaino, G. Sheerin, D. Carty, T. McEvoy, C. Barnes, V. Dhanak, and A. Santoni, Surf. Sci. **544**, 121 (2003).

[6] J. Martínez-Blanco, V. Joco, P. Segovia, T. Balasubramanian, and E. G. Michel, Appl. Surf. Sci. **252**, 5331 (2006).

[7] J. Martínez-Blanco, V. Joco, J. Fujii, P. Segovia, and E. G. Michel, J. Phys.: Condens. Matter **21**, 055001 (2009).

[8] S. H. Overbury and Y.-S. Ku, Phys. Rev. B **46**, 7868 (1992).

[9] A. K. Schmid, N. C. Bartelt, and R. Q. Hwang, Science **290**, 1561 (2000).

[10] F. Reinert, G. Nicolay, S. Schmidt, D. Ehm, and S. Hüfner, Phys. Rev. B **63**, 115415 (2001).

[11] G. Le Lay, V. Yu. Aristov, O. Boström, J. M. Layet, M. C. Asensio, J. Avila, Y. Huttel, and A. Cricenti, Appl. Surf. Sci. **123-124**, 440 (1998).

[12] R. I. G. Uhrberg and T. Balasubramanian, Phys. Rev. Lett. **81**, 2108 (1998).

[13] K. Hermann and M. A. van Hove, "LEEDpat," [http://www.fhi-berlin.mpg.de/KHsoftware/LEEDpat/index.html], accessed on September 15, 2010.

[14] J. J. Barton, S. W. Robey, and D. A. Shirley, Phys. Rev. B **34**, 778 (1986).

[15] S. Y. Tong, H. Li, and H. Huang, Phys. Rev. B **46**, 4155 (1992).

[16] V. Fritzsche and D. P. Woodruff, Phys. Rev. B **46**, 16128 (1992).

[17] P. S. Mangat, P. Soukiassian, K. M. Schirm, L. Spiess, S. P. Tang, A. J. Freeman, Z. Hurych, and B. Delley, Phys. Rev. B **47**, 16311 (1993).

[18] H. Wu, G. J. Lapeyre, H. Huang, and S. Y. Tong, Phys. Rev. Lett. **71**, 251 (1993).

[19] M. T. Sieger, D. A. Luh, T. Miller, and T.-C. Chiang, Phys. Rev. Lett. **77**, 2758 (1996).

[20] C. Yu, J. Liu, H. Lu, and J. Chen, Appl. Surf. Sci. **253**, 8652 (2007).